



Large magnetoresistance and unexpected low thermal conductivity in topological semimetal CrP₄ single crystal

HPSTAR
1379-2022

W. Wu¹ · Z. H. Yu² · M. Xu³ · X. L. Liu² · J. G. Zhao⁴ · Z. Y. Liu¹ · W. Xia² · Z. Y. Li² · C. Y. Zhou⁵ · J. J. Feng⁶ · M. Xu³ · Y. F. Guo² · J. L. Luo¹

Received: 26 September 2021 / Accepted: 20 January 2022
© The Author(s), under exclusive licence to Springer-Verlag GmbH, DE part of Springer Nature 2022

Abstract

We fabricate CrP₄ single crystal under high pressure and high temperature at 5 GPa and 1373 K. The comprehensive physical properties including electronic transport, magnetic properties, specific heat, Hall, thermal Seebeck and thermal conductivity are reported here. The resistivity shows a good metallic conductivity and $T^{2.7}$ law relation in the low temperature, which indicates a weak correlation of electrons. It is interesting to note that CrP₄ shows large magnetoresistance (MR) of 500% under $T=2$ K and $B=9$ T, and the MR does not reach saturation until 9 T. The mechanism of large MR in CrP₄ is interpreted as the Fermi surface anisotropy. The Hall measurement shows that there is only one single type of carriers in CrP₄ with holes. CrP₄ exhibits paramagnetic behavior observed from the magnetic susceptibility measurement. Though CrP₄ exhibits high electrical conductivity, unexpected low thermal conductivity is observed at low temperature, which is due to the zigzag chain of CrP₆ octahedra along the c -axis. Low thermal conductivity is useful to design thermoelectric materials or devices by properly doping in CrP₄.

Keywords Transition metal phosphide · High pressure and high temperature synthesis · Magnetoresistance · Thermal conductivity

W. Wu, Z. H. Yu and M. Xu have contributed equally to this work.

- ✉ W. Wu
welyman@iphy.ac.cn
- ✉ Z. H. Yu
yuzhh@shanghaitech.edu.cn

- ¹ Beijing National Laboratory for Condensed Matter Physics and Institute of Physics, Chinese Academy of Sciences, Beijing 100190, China
- ² School of Physical Science and Technology, ShanghaiTech University, Shanghai 201210, China
- ³ Wuhan National Laboratory for Optoelectronics, School of Optical and Electronic Information, Huazhong University of Science and Technology, Wuhan, 430074, China
- ⁴ School of Physics, Harbin Institute of Technology, Harbin 150080, China
- ⁵ Shanghai Synchrotron Radiation Facility, Shanghai Advanced Research Institute, Chinese Academy of Sciences, Shanghai, 201204, China
- ⁶ Center for High Pressure Science and Technology Advanced Research, Shanghai 201203, China

1 Introduction

Transition metal pnictides (such as phosphides and arsenides) represent an important class of binary and ternary compounds with a wide diversity of composition, crystal structure and physical properties such as high magnetoresistance (MR) and superconductivity. From the chemical viewpoint, transition metal pnictides could be divided into metal-rich pnictides such as Mo₃P [1] and Cr₂As [2], monopnictides such as CrAs [3] and MnP [4] as well as pnictogen-rich pnictides such as NiP₂ [5], Nb₂P₅ [6, 7] and SrAs₃ [8]. Phosphorus-rich phosphides were investigated far less extensively in the literature in contrast to their metal-rich counterparts [9]. This may be due to the difficulty in preparing samples using conventional ambient-pressure and high-temperature techniques in overcoming the large difference of melting point between phosphorus and transition metal, as well as the high vapor pressure of phosphorus under high temperature. The high-pressure and high-temperature (HPHT) technique has been demonstrated to be useful in preparing these phosphorus-rich phosphides materials such as CrP₂ [10], CoP₃ [11] and CrP₄ [12]. The Cr-based compounds, especially, Cr-based superconductors

have attracted considerable interests due to the $3d$ electron correlation and antiferromagnetic fluctuation leading to novel and unconventional superconductivity [13, 14], the investigation on physical properties of Cr-based phosphides systems is important and interesting, which often leads to new discoveries.

Recently, transition metal pnictides (such as TaP_2 , TaAs_2 , MoP_2 and WP_2) have attracted a lot of attentions owing to their extremely large magnetoresistance (XMR) [15, 16], which is attributed to their nearly perfectly compensated electrons and holes carriers according to both band structure calculations and angle-resolved photoemission spectroscopy (ARPES) measurements [17]. Very recently, CrP_4 was predicted as a high symmetry line semimetal according to the catalog of topological electronic materials in Weng's recent investigation [18]. In Ref. [12], the authors measured the magnetic properties and electrical transport of CrP_4 single crystal. However, other physical properties such as magnetic transport properties, carrier type, specific heat and thermal conductivity were not reported in the literature. Yet, these properties are important to fully understand the physical properties of CrP_4 and related transition metal pnictides.

In this paper, we systematically measured the electrical transport, Hall effect, thermal Seebeck, thermal conductance and magnetic properties of CrP_4 . The present resistivity of CrP_4 shows a good metallic conductivity and $T^{2.7}$ law relation in low temperature, which indicates a weak correlation of electrons. In most cases, nonmagnetic metallic materials exhibit feeble or small MR. However, it is interesting to note that the MR of CrP_4 at $T=2$ K and $B=9$ T goes to 500%. In addition, the MR follows a $H^{1.4}$ law relation and does not reach saturation until 9 T. The aforementioned characters of MR in CrP_4 resemble the recently discovered topological semimetals, which guides us to explore the mechanism of large MR in CrP_4 . In addition, the Hall effect measurement is important to investigate the carrier type, which could provide the information for exploring the mechanism of MR as well as the band structure near the Fermi surface of CrP_4 . The remarkable MR in recently reported transition metal pnictides is interpreted as the compensated electrons and holes. However, CrP_4 has only one type of carriers (holes). Therefore, the mechanism of large MR in CrP_4 is different from the aforementioned topological semimetals. Generally speaking, metallic compounds show high thermal conductivity because the charge carriers simultaneously transmit the heat. However, the present CrP_4 , which shows metallic behavior, surprisingly exhibits low thermal conductivity.

2 Experimental and theoretical details

2.1 Single crystal growth using multi-anvil apparatus (MAA)

CrP_4 single crystals were grown by reacting Cr and red phosphorus powder under HPHT conditions in a Kawai-type MAA. The mixture of Cr and P powders in a mole ratio of about 1:5 was compressed into a cylinder and placed in a hexagonal boron nitride (h-BN) cell with a size of 3.5 mm in inner diameter and 3.2 mm in depth. The assembly was first pre-compressed under a pressure of 5.0 GPa and was then heated up to 1100 °C for 30 min with maintaining the pressure. After a reaction for 2 h at this pressure and temperature, the sample was slowly cooled down to 900 °C within 2 h, followed by quenching to room temperature by turning off the electrical power supply without releasing the pressure. The pressure was finally gradually released at room temperature.

2.2 Crystal structure characterization

The crystallographic phase and quality examinations of CrP_4 were performed on a Bruker D8 single-crystal X-ray diffractometer (SXRD) with $\text{Mo } K_{\alpha 1}$ ($\lambda = 0.71073$ Å) at 298 K. The powder XRD was carried on a Bruker D2 diffractometer with Cu radiation ($\lambda = 1.5418$ Å) at 298 K. The structure refinement was refined by the Rietveld method using FullProf [19].

2.3 Physical properties measurement under low temperature

The electrical resistivity and specific heat were measured in a quantum design physical property measurement system (PPMS-9) by the standard four electrodes method and relaxation method, respectively. The Hall effect measurements were carried out using a standard Hall bar geometry in a PPMS. The direct current (DC) magnetization was measured in a magnetic property measurement system (MPMS). The Seebeck and thermal conductivity was measured together in the PPMS. The puck and software are designed by ourselves.

2.4 First-principles calculations

The density functional theory (DFT) simulations were carried out using the Vienna Ab initio Simulation Package (VASP) [20]. The generalized gradient approximation (GGA) in the form of Perdew–Burke–Ernzerhof (PBE) was used [21]. The energy cutoff for the plane waves was set to 500 eV. The criteria for self-consistent iterations were

10^{-7} eV for electronic steps and 10^{-6} eV for ionic steps. The experimental crystal structure was used for the band structure and Fermi surface plotting. Our test of the structural relaxation gives qualitatively the same results. For plotting the band structure, we used a dense Brillouin zone sampling along the k -paths (2500 k -points) and find that the energy gap along A–G still exists [22]. The Fermi surface was visualized using the XcrysDen tool.

3 Results and discussion

3.1 Single crystal analysis and crystal structure

The small and bright reciprocal space diffractions without any other miscellaneous points, seen in Fig. 1a–c, indicate the high quality of the CrP_4 single crystal as-prepared in the present work. The crystal structure of CrP_4 is determined from three dimensional single crystal counter data, and it crystallizes into monoclinic structure (space group $C2/c$, No. 15) with lattice parameter of $a = 5.1944$ Å, $b = 10.7736$ Å, $c = 5.7758$ Å, $\beta = 110.606^\circ$, which is consistent with the

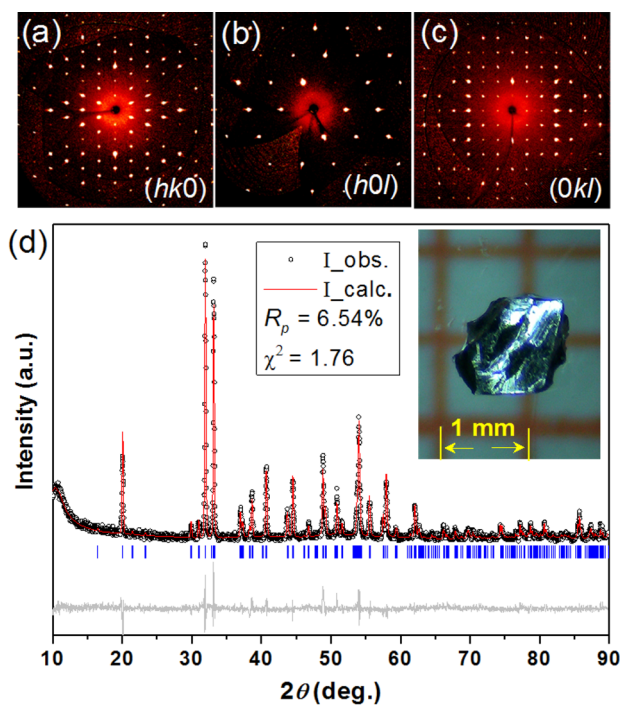


Fig. 1 a–c Diffraction patterns in the reciprocal space along $(hk0)$, $(h0l)$ and $(0kl)$ directions. **d** Powder XRD pattern of pulverized CrP_4 single crystals measured at room temperature. The observed (black open circle) and calculated (red solid line) profiles are shown on the top. The blue vertical marks in the middle are calculated positions of the Bragg peaks. The gray line at the bottom is the difference between calculated and observed intensities. Inset shows the refinement residual factor and optical image of CrP_4 single crystal

previous work ($a = 5.1914$ Å, $b = 10.7600$ Å, $c = 5.7712$ Å and $\beta = 110.648^\circ$) [12]. Furthermore, Rietveld refinement of powder XRD pattern for pulverized CrP_4 single crystals measured at room temperature also confirm the sample with good crystallographic quality (see Fig. 1d). The optical image of CrP_4 single crystal with size of $\sim 1 \times 1$ mm is shown in inset of Fig. 1d.

CrP_4 belongs to the monoclinic VP_4 -type structure as shown in Fig. 2a. In Fig. 2b, the Cr^{2+} cations are sandwiched between the P_4^{2-} anions, so that one Cr^{2+} layer and two armchair-like P_4^{2-} layers alternatively stack along the b -axis. The structure of CrP_4 has Cr chains with uniform intrachain separation of 3.18 Å and interchain distance of 5.19 Å, as shown in Fig. 2c. The Cr atom is coordinated by six P atoms, forming a distorted CrP_6 octahedron. The CrP_6 octahedra share edges, forming zigzag chains along the c -direction (see Fig. 2d). These crystallographic characters suggest that CrP_4 is a quasi-one-dimensional (1D) material. Since CrP_4 exhibits this quasi-1D crystal structure character and metallic transport behavior, it might be expected to show charge density wave driven instabilities. Moreover, the zigzag chain

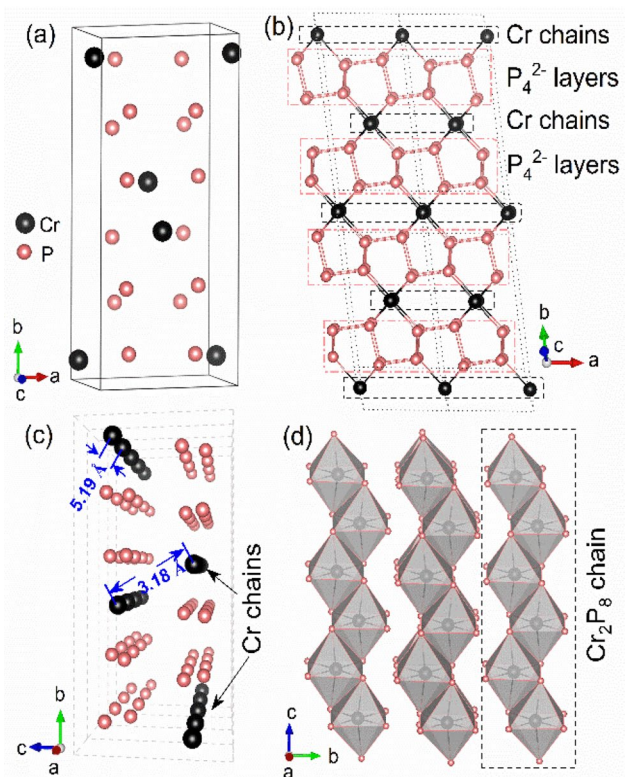


Fig. 2 **a** The crystal structure of CrP_4 crystallizing into monoclinic lattice with space group $C2/c$. **b** The Cr chains were sandwiched between the P_4^{2-} layers along b -axis. **c** The structurally quasi-one dimensional Cr chains along a -axis in CrP_4 . **d** The Cr atoms were coordinated with six P atoms forming CrP_6 octahedron, which shares edges forming Cr_2P_8 chains along c -axis

in CrP₄ will give rise to an important great effect on the thermal conductivity.

3.2 Electrical transport and MR effect

Detailed measurements of electrical transport and magnetic properties of CrP₄ single crystal have not been previously carried out during 1.8–4.2 K. Figure 3a, b shows a complete summary of experimental results for CrP₄ including resistivity and MR. Figure 3a shows the temperature dependence of resistivity for CrP₄ at zero magnetic field. CrP₄ exhibits metallic behavior which means that it is an itinerant system. At high temperature, the resistivity of CrP₄ tends to level off. The present resistivity of CrP₄ shows a good metallic conductivity and $T^{2.7}$ law relation (see inset of Fig. 3a) in the low temperature, which indicates a weak correlation of electrons. From Fig. 3b, we could found that CrP₄ has MR of 500% at $T \sim 1.8$ K and $B = 9$ T. Magnetic field dependence of MR exhibited a 1.4 power relation. Figure 3b shows the magnetic field dependence of MR at selected temperatures

(2 K, 100 K and 200 K), in which the MR was enhanced as the temperature decreases.

Generally speaking, nonmagnetic metallic materials exhibited feeble or small MR. As shown in Fig. 3b, CrP₄ exhibits metallic behavior as the temperature decreases. However, herein CrP₄ shows large MR of 500% under $T = 2$ K and $B = 9$ T. The MR at 2 K as a function of temperature shows quadratic parabola behavior. The MR does not reach saturation up to 9 T and will not come into saturation even up to very high magnetic field. These character of MR in CrP₄ observed here is similar with the recently discovered topological semimetals. Large MR is a typical feature of compensated semimetals such as TaAs₂ (MR = $1.2 \times 10^6\%$ at $B = 9$ T and $T = 2$ K) [15] and TaP₂ (MR = 700% at $B = 9$ T and $T = 2$ K) [16] and Bi [23]. The mechanism of large MR in semimetals such as TaAs₂ is interpreted as compensated electron and hole. We conducted further experimental and theoretical investigation to verify whether the physical mechanism of large MR in CrP₄ stems from the compensation of electrons and holes. Since different materials

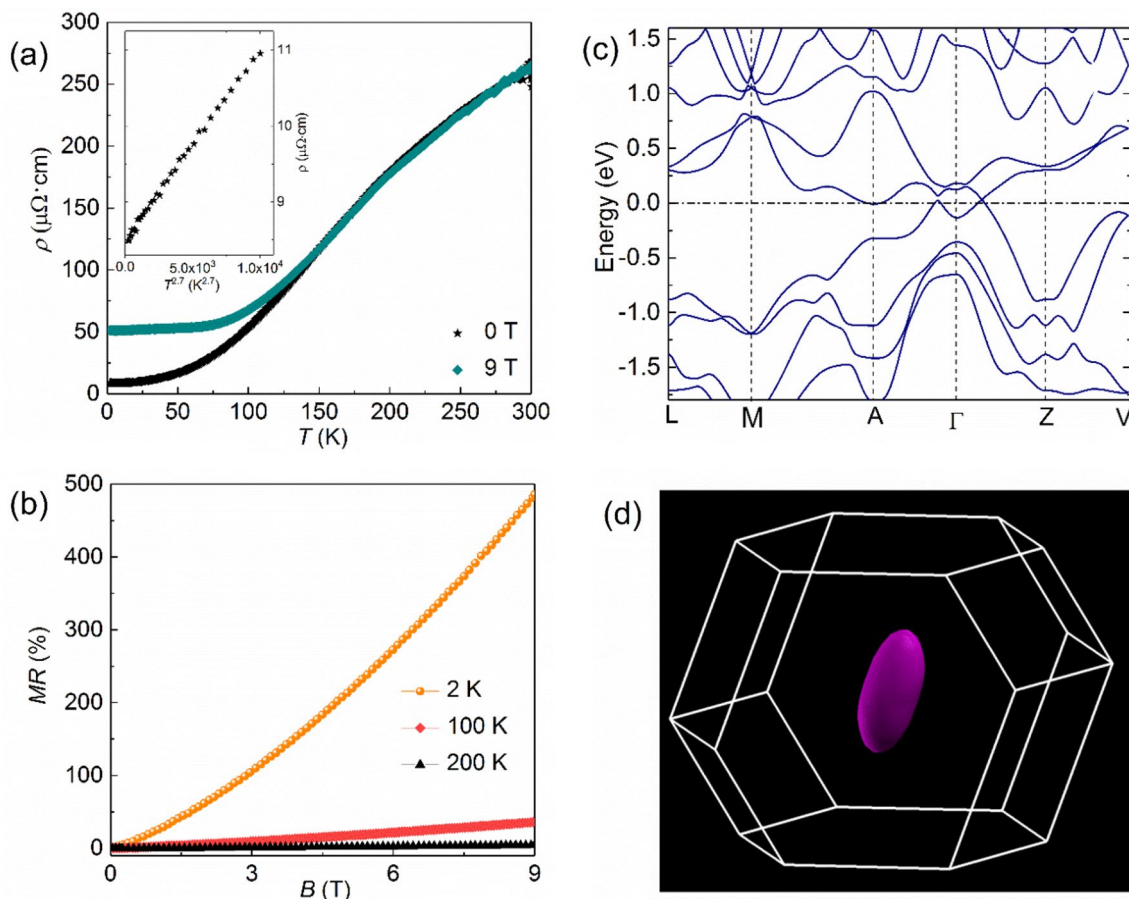


Fig. 3 **a** Temperature dependence of the resistivity. The resistivity as a function of temperature was mathematically fitted and yielded a 2.7 power law [inset of (a)]. **b** Magnetic field dependence of MR at

selected temperatures (2 K, 100 K and 200 K). **c**, **d** The band structure and Fermi surface of CrP₄

(especially ferromagnetic and antiferromagnetic) have different mechanisms for interpreting large MR, we herein mainly focus on the MR in nonmagnetic materials (such as the present CrP₄). The most common metal copper (Cu) has positive MR of 800% (4.2 K) [24]. Graphene has MR = 100% at 2 K and 14 T [25]. The semimetal WTe₂ exhibited exotic longitudinal linear magnetoresistance with MR = 1200% at 2 K and 15 T [26]. The main mechanism of these large MR in nonmagnetic materials is the Fermi surface anisotropy. To interpret the large MR in CrP₄, we investigate the Fermi surface of CrP₄ by performing DFT simulations. The band structure and Fermi surface of CrP₄ are shown in Fig. 3c, d. The Fermi level falls in the energy bands, indicating a metallic behavior, which is consistent with the experimental electrical transport measurement. The energy bands near the Fermi level are more dispersed in the energy from -1 to 0 eV and show the character of linear dispersion. The Fermi surface of CrP₄ is shown in Fig. 3d, from which we observed a small and anisotropic Fermi surface. The density of state (DOS) around the E_F level is about 2 states/eV. The present first-principles calculation results are in good agreement with the Refs. [27, 28].

3.3 Hall effect measurement

To fully address the physical mechanism of large MR in CrP₄, we studied the Hall effect as a function of magnetic field at selected temperatures, which could determine the carrier type, density and carrier mobility. The magnetic field dependence of Hall resistivity ρ_{xy} for CrP₄ presented in Fig. 4 exhibits roughly linear trend at temperatures during 2 K and 300 K, indicating that only hole carriers participate

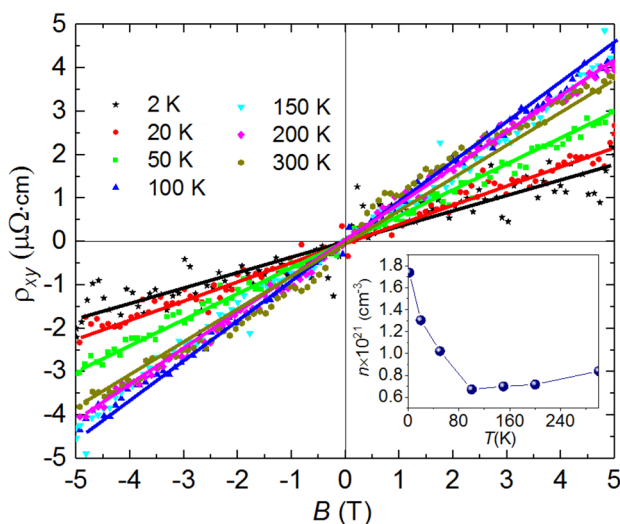


Fig. 4 Hall resistivity versus magnetic field B for CrP₄ at different temperatures, the solid line are the linear fitted results for eye guide. The inset shows the temperature dependence of carrier density

in the transport. For the transition metal pnictides such as TaP₂, NbAs₂, etc. The field dependence of Hall resistivity ρ_{xy} exhibits large deviation from the linearity at low temperature, indicating that both electron and hole carriers participate in the transport. Therefore, the mechanism of large MR in CrP₄ is different from the topological semimetals such as TaAs₂ and TaP₂. The carrier density of CrP₄ increases as the temperature decreasing as shown in inset of Fig. 4. The carrier density data are temperature and sample independent and fall in the typical 10^{20} – 10^{21} cm⁻³ range for semimetals, which accounts for bad metallic properties of the compound. The recently discovered semimetals also have low carrier density, high carrier mobility and small effective mass, and thus, a moderate magnetic field can drive these materials into the quantum regime. There is a large scatter in the Hall resistivity data at low temperatures (particularly 2 K) due to the irregular shape of the HPHT CrP₄ sample.

3.4 Magnetic susceptibility and Bader charge

Jeitschko and Donohue reported that CrP₄ is Pauli paramagnetic [12]. Magnetic measurements between 4.2 K and room temperature showed no detectable magnetic moment indicating diamagnetic or Pauli paramagnetic. In Fig. 5, we plot the DC magnetic susceptibility curves for the present single crystal of CrP₄ as a function of temperature, which exhibits paramagnetism in a broad range near room temperature. The reasonable experimental intrinsic susceptibility range is about 1×10^{-6} emu/g Oe to 2×10^{-7} emu/g Oe. The calculated susceptibility χ is 4×10^{-7} emu/g Oe according to the formula of $\chi = \mu_0 \mu_B^2 N(E_F)$. This value roughly agrees with the experimental susceptibility result.

From the crystallographic viewpoint, the crystalline structure of the CrP₄ exhibits the layered stacking of the black phosphorus in which the metal atoms Cr are inserted between two buckled phosphorus layers [29]. The two type nonequivalent P atoms (nominated as P(1) and P(2)) in CrP₄ are tetrahedrally coordinated to other P atoms and Cr atoms (as shown in inset of Fig. 5a). Such compounds can be rationalized on the basis of classical two electrons bonds [30]. By counting two electrons for each of the short near-neighbor interactions, the Cr atoms obtain the oxidation number 2+. Thus, the electronic configuration of Cr in CrP₄ is $3d^4$, which means that Cr²⁺ is a nonmagnetic ion. To verify our above mentioned oxidation state of Cr in CrP₄, we performed first-principles calculations to simulate the Bader charge of CrP₄. It is found from Fig. 5b that the electrons transfer from Cr to P atoms, which is consistent with our speculation.

As shown in Fig. 5, the ELF shows P–P bonds are fully covalent, as the electrons are localized in the middle of two atoms. Meanwhile the electrons of Cr–P bonds are closer to P, indicating stronger ionicity. Then, we calculated Bader

Fig. 5 **a** Magnetic susceptibility of CrP₄. The inset of upper-right panel shows the atomic neighbor for P(1) and P(2), respectively. CN and ON are short for coordination number and oxidation number, respectively. The lower right inset is the CrP₆ octahedra sharing edge. **b** Bader charge of CrP₄

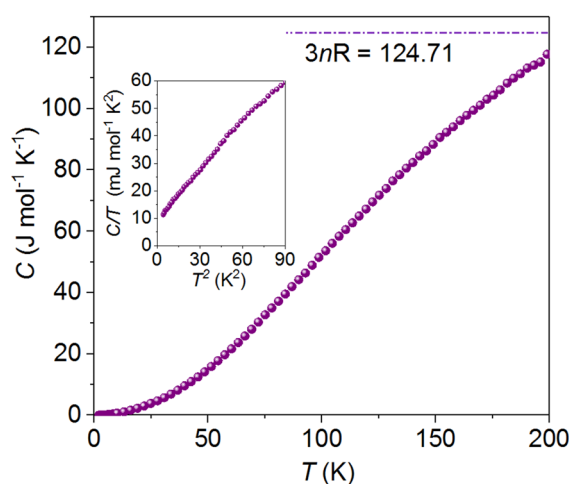
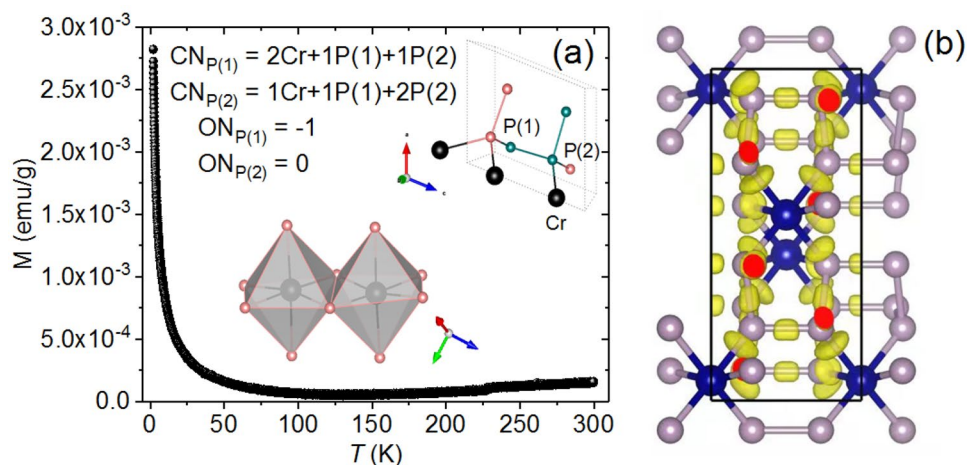


Fig. 6 Specific heat of CrP₄. The inset shows the T^2 dependence of C divided by T (C/T)

charge distribution to quantize the electron transfer. It shows that Cr has 5.33 electrons, and P has 5.25 or 5.08 averagely, and thus, each Cr atom gives ~ 0.67 electron to P.

3.5 Specific heat

The heat capacity measurement was carried out to reveal the physical properties of CrP₄. Figure 6 shows the temperature-dependent specific heat, $C(T)$. No anomalies are found in the whole measured range (2–200 K), which indicates the absence of first-order phase transitions. At room temperature, the heat capacity reaches the value expected by Dulong–Petit law $3nR = 124.71$ J/mol K, where R is a gas constant ($R = 8.31$ J/mol K), and n is the number of atoms per formula unit.

Low temperature (2–30 K) data of specific heat divided by T (C/T) versus T^2 ($C/T = \gamma T + \beta T^2$) are presented in the inset of Fig. 6, where γ is the Sommerfeld coefficient, and

β is the phonon specific heat parameter. The first term γT represents an electronic contribution, and βT^3 is the phonon contribution to the specific heat. By fitting the low temperature data below 8 K, we obtain $\gamma = 10$ mJ K⁻² mol⁻¹ and $\theta_D = 311(5)$ K. This γ value is similar with CrP which have a valley of the density of states (DOS) at the Fermi level. The calculated γ value is 4.9 mJ K⁻² mol⁻¹ according to the DOS of CrP₄. The calculated and experimental results of γ are roughly consistent. The differences between the experimental and theoretical values stem from several factors such as the theoretical calculation parameters (exchange–correlation function, pseudopotential), the imperfection of quality for single crystal as well as the divergence of temperature in DFT calculation (0 K) and experimental measurement (≥ 2 K).

3.6 Thermal conductivity

Figure 7a shows the Seebeck thermopower of CrP₄ as a function of temperature, from which we find that the coefficient of Seebeck effect is positive, indicating that holes are the main charge carriers. The thermopower increases linearly within the whole temperature range, achieving 11 μ V/K at room temperature. The carrier concentration and Fermi energy level position of metals are basically independent of temperature, thus the Seebeck thermopower of metals must be very small. Generally, the Seebeck coefficient is 0–10 μ V/K. The mechanism of Seebeck effect in CrP₄ probably correlated with the influence of electron free path.

Normally, metallic compounds show high thermal conductivity because the charge carriers are simultaneously responsible for thermal conductivity. However, the present CrP₄, which shows metallic behavior, surprisingly exhibits low thermal conductivity (below 1 W/m K), especially in the low temperature (see Fig. 7b). The thermal conductivity firstly shows rapid increase from 10 to 60 K and then increases slowly as the temperature further increasing,

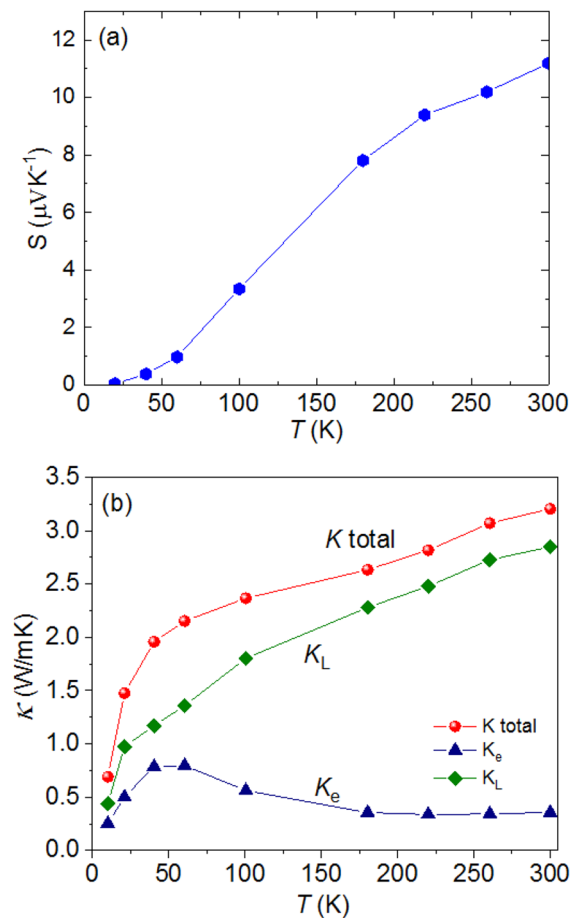


Fig. 7 **a** Temperature dependence of Seebeck thermopower. **b** Temperature dependence of thermal conductivity in CrP_4 , in which the total thermal conductivity was fitted with lattice and electron contribution

reaching 3.2 W/mK at room temperature. The total thermal conductivity (K) was fitted with lattice (K_L) and electron (K_e) contributions as shown in Fig. 7b. We estimate the electronic contribution for thermal conductivity K_e , which is related to the electrical conductivity σ ($\sigma = 1/\rho$) through the Wiedemann–Franz (WF) law ($K_e = L_0\sigma T$), where L_0 is a universal constant known as the Sommerfeld value of the Lorenz number. The K_L and K_e show roughly equal contribution to thermal conductivity at low temperature (≤ 60 K). The K_L becomes the main part as the temperature further increasing (≥ 60 K).

The low thermal conductivity phenomena were also observed in other metal phosphides such as the filled skutterudite such as CoP_3 . One proposed model that could explain low thermal conductivity in CoP_3 is the so-called rattling effect [11]. Great efforts, thus, have been made to clarify the origin of this low thermal conductivity. The Cr atom is coordinated by six P atoms, forming a distorted CrP_6 octahedron. The CrP_6 octahedra share edges, forming zigzag

chains along the c -direction (as shown in Fig. 2d). We suggested that this crystallographic zigzag chain character is the main factor for affecting the thermal conductivity. However, it should be noted that quasi-1D structural unit is not a requirement for the low thermal conductivity, but the zigzag chains in some materials play an importance role in low thermal conductivity such as SeSn .

4 Conclusion

We have prepared the single crystal of CrP_4 using HPHT technique and carefully measured the electrical transport and magnetic properties, Hall effect, specific heat and thermal Seebeck. The resistivity of CrP_4 shows a good metallic conductivity and $T^{2.7}$ law relation in the low temperature which indicates a weak correlation of electrons. Our key finding is that the large MR of 500% is observed at $T = 2$ K and $B = 9$ T, which has an $H^{1.4}$ law relation with magnetic field. The present Hall effect measurement suggested CrP_4 has only one single type carrier with hole, which is different from the recently discovered semimetals with equal electron/hole density and mobility. Paramagnetic behavior was observed from the magnetic susceptibility. Those properties are corresponding to the topology semimetal like other these compounds. Another noteworthy finding we reported here is that CrP_4 exhibited very low thermal conductivity due to CrP_6 octahedra zigzag chain along c -axis.

Acknowledgements The authors acknowledge the support by the Major Research Plan of the National Natural Science Foundation of China (No. 92065201). W. Wu acknowledges National Key Research and Development of China (Grant Nos. 2017YFA0302901 and 2017YFA0302903), the National Natural Science Foundation of China (Grant Nos. 12134018, and 11921004), the Strategic Priority Research Program of the Chinese Academy of Sciences (Grant No. XDB33010100) Y. F. G. acknowledges the start-up grant of ShanghaiTech University and the Program for Professor of Special Appointment (Shanghai Eastern Scholar). M. Xu acknowledges the Fundamental Research Funds for the Central Universities, HUST (No. 2021GCRC051)

Declarations

Conflict of interest The authors declare that they have no conflict of interest.

References

1. A.O. Oliyanyk, Y.F. Lomnytska, M.V. Dzevenko, S.S. Stoyko, A. Mar, *Inorg. Chem.* **52**, 983 (2013)
2. Z.H. Yu, C.Y. Li, H.Z. Liu, *Solid State Commun.* **152**, 509 (2012)
3. Z.H. Yu, W. Wu, J.G. Zhao, C.Y. Li, J.G. Cheng, J.L. Luo, L. Wang, H.K. Mao, *P. Natl. Acad. Sci. USA* **112**, 14766 (2015)
4. J.G. Cheng, K. Matsubayashi, W. Wu, J.P. Sun, F.K. Lin, J.L. Luo, Y. Uwatoko, *Phys. Rev. Lett.* **114**, 117001 (2015)

5. B. Owens-Baird, J.Y. Xu, D.Y. Petrovykh, O. Bondarchuk, Y. Ziouani, N. González-Ballesteros, P. Yox, F.M. Sapountzi, H. Niemantsverdriet, Y.V. Kolenko, K. Kovnir, *Chem. Mater.* **31**, 3407 (2019)
6. R. Kanno, N. Kinomura, M. Koizumi, S. Nishigaki, K. Nakatsu, *Acta Cryst. B* **36**, 2206 (1980)
7. X.L. Liu, Z.H. Yu, Q.F. Liang, C.Y. Zhou, H.Y. Wang, J.G. Zhao, X. Wang, N. Yu, Z.Q. Zou, Y.F. Guo, *Chem. Mater.* **32**, 8781 (2020)
8. E.J. Cheng, W. Xia, X.B. Shi, Z.H. Yu, L. Wang, L.M. Yan, D.C. Peets, C.C. Zhu, H. Su, Y. Zhang, D.Z. Dai, X. Wang, Z.Q. Zou, N. Yu, X.F. Kou, W.G. Yang, W.W. Zhao, Y.F. Guo, S.Y. Li, *NPJ Quantum Mater.* **5**, 38 (2020)
9. H. Georg, V. Schnering, W. Hoenle, *Chem. Rev.* **88**, 243 (1988)
10. W. Jeitschko, P.C. Donohue, *Acta Cryst. B* **29**, 783 (1973)
11. C.H. Lee, H. Kito, H. Ihara, K. Akita, N. Yanase, C. Sekine, I. Shirotnani, *J. Cryst Growth* **263**, 358 (2004)
12. W. Jeitschko, P.C. Donohue, *Acta. Cryst. B* **28**, 1893 (1972)
13. W. Wu, J.G. Cheng, K. Matsubayashi, P.P. Kong, F.K. Lin, C.Q. Jin, N.L. Wang, Y. Uwatoko, J.L. Luo, *Nat. Commun.* **5**, 5508 (2014)
14. W. Wu, K. Liu, Y.J. Li, Z.H. Yu, D.S. Wu, Y.T. Shao, S.H. Na, G. Li, R.Z. Huang, T. Xiang, J.L. Luo, *Natl. Sci. Rev.* **7**, 21 (2020)
15. D.S. Wu, J. Liao, W. Yi, X. Wang, P.G. Li, H.M. Weng, Y.G. Shi, Y.Q. Li, J.L. Luo, X. Dai, Z. Fang, *Appl. Phys. Lett.* **108**, 042105 (2016)
16. H.Y. Wang, H. Su, J.Y. Zhang, W. Xia, Y.S. Lin, X.L. Liu, X.F. Hou, Z.H. Yu, N. Yu, X. Wang, Z.Q. Zou, Y.H. Wang, Q.F. Liang, Y.H. Zhen, Y.F. Guo, *Phys. Rev. B* **100**, 115127 (2019)
17. M.Y. Yao, N. Xu, Q.S. Wu, G. Autès, N. Kumar, V.N. Strocov, N.C. Plumb, M. Radovic, O.V. Yazyev, C. Felser, J. Mesot, M. Shi, *Phys. Rev. Lett.* **122**, 176402 (2019)
18. T.T. Zhang, Y. Jiang, Z.D. Song, H. Huang, Y.Q. He, Z. Fang, H.M. Weng, C. Fang, *Nature* **566**, 475 (2019)
19. J. Rodríguez-Carvajal, *Phys. B* **192**, 55 (1993)
20. G. Kresse, J. Furthmüller, *Phys. Rev. B* **54**, 11169 (1996)
21. J.P. Perdew, Y. Wang, *Phys. Rev. B* **45**, 13244 (1992)
22. H.J. Monkhorst, J.D. Pack, *Phys. Rev. B* **13**, 5188 (1976)
23. F.Y. Yang, K. Liu, K. Hong, D.H. Reich, P.C. Searson, C.L. Chien, *Science* **284**, 1335 (1999)
24. A.J. Funes, R.V. Coleman, *Phys. Rev.* **131**, 2084 (1963)
25. Z.M. Liao, H.C. Wu, S. Kumar, G.S. Duesberg, Y.B. Zhou, Graham L.W. Cross, I.V. Shvets, D.P. Yu, *Adv. Mater.* **24**, 1862 (2012)
26. Y.F. Zhao, H.W. Liu, J.Q. Yan, W. An, J. Liu, X. Zhang, H.C. Wang, Y. Liu, H. Jiang, Q. Li, Y. Wang, X.Z. Li, D. Mandrus, X.C. Xie, M.H. Pan, J. Wang, *Phys. Rev. B* **92**, 041104(R) (2015)
27. N. Gong, C.X. Deng, L.L. Wu, B. Wan, Z.B. Wang, Z.P. Li, H.Y. Gou, F.M. Gao, *Inorg. Chem.* **57**, 9385 (2018)
28. M.R. Khan, K. Bu, J.S. Chai, J.T. Wang, *Sci. Rep.-UK* **10**, 11502 (2020)
29. A. Brown, S. Rundqvist, *Acta Crystallogr.* **19**, 684 (1965)
30. F. Hulliger, E. Mooser, *Prog. Solid State Chem.* **2**, 330 (1965)

Publisher's Note Springer Nature remains neutral with regard to jurisdictional claims in published maps and institutional affiliations.